

# Ultrasensitive hydrogen detection by electrostatically formed silicon nanowire decorated by palladium nanoparticles

Anwasha Mukherjee <sup>a,\*</sup>, Mohamad Gnaim <sup>a, ¶</sup>, Idan Shem Tov <sup>a, ¶</sup>, Laura Hargreaves <sup>b</sup>, Joseph Hayon <sup>a</sup>, Alexander Shluger <sup>b</sup>, and Yossi Rosenwaks <sup>a,\*</sup>

<sup>a</sup>Department of Physical Electronics, School of Electrical Engineering, Tel Aviv University, Ramat Aviv – 69978, Israel

<sup>b</sup>London Centre for Nanotechnology and Department of Physics and Astronomy, University College London, Gower Street, London WC1E 6BT, UK

Email: [anwesham@mail.tau.ac.il](mailto:anwesham@mail.tau.ac.il)

[yossir@eng.tau.ac.il](mailto:yossir@eng.tau.ac.il)

## Abstract

Developing high performance hydrogen (H<sub>2</sub>) sensors is of utmost importance to facilitate the safe usage of H<sub>2</sub> as the alternative source of clean and renewable energy. We present an ultra-sensitive H<sub>2</sub> sensor operating in air and based on electrostatically formed nanowire (EFN) sensor decorated by palladium nanoparticles (Pd NPs). By appropriate tuning of the various gate voltages of the EFN, an extremely high sensor response of  $\sim 2 \times 10^6$  % (0.8% H<sub>2</sub> exposure) and a sensitivity of  $\sim 400$  % ppm<sup>-1</sup> is obtained at room temperature (20±2 °C). This sensor outperforms, to the best of our knowledge, most of the reported resistive and field effect transistor (FET) based H<sub>2</sub> sensors. The EFN power consumption varies from few pW to  $\sim 436$  nW at maximum current operation thus enabling ultra-low power usage at room temperature. In addition, the sensor exhibits fast response and recovery times, retains good sensing performances even at 50% relative humidity (RH) and

exhibits reproducibility over time. Combining Pd NPs with the unique features of the EFN platform makes Pd-EFN a versatile, robust, low power, rapid, and highly sensitive H<sub>2</sub> sensor.

*Keywords:* Electrostatically formed silicon nanowire, Palladium nanoparticles, Hydrogen sensing, Kelvin probe force microscopy

## 1. Introduction

Hydrogen (H<sub>2</sub>) is one of the most promising sources of clean and renewable energy [1,2]. Due to its high energy density of 120-142 MJ kg<sup>-1</sup> (almost three times that of fossil fuels), significant heat of combustion, zero carbon emission, and reducing capabilities, H<sub>2</sub> finds widespread applications in fuel cells of electric vehicles [2–5], metal reduction, chemical industry, petroleum extraction and more [2,6]. However, due to its ultra-small molecule size (lowest atomic number), low ignition energy (0.02 mJ), large flame propagation velocity, wide flammable range (4-75%) and high diffusion coefficient in air (0.6 cm<sup>2</sup>/s), H<sub>2</sub> have an increased risk of explosions during production, transportation, storage and usage [2,5,6]. Thus, safe usage of H<sub>2</sub> as the next generation fuel demands high performance H<sub>2</sub> gas sensors with high sensitivity, selectivity and fast dynamics, to timely detect and monitor H<sub>2</sub> leaks even at low concentrations (less than the lower explosive limit of 4%), in order to prevent explosions and fatalities. It is also desirable that these H<sub>2</sub> sensors should maintain their performances under ambient conditions, consume minimum power, and should be manufactured at a very large scale for wide applications.

H<sub>2</sub> sensors based on metal oxide semiconductors have been widely reported [7–10]. However, most of them operate at high temperatures (200 to 500°C) which consumes power and may lead to explosion. Hence, deposition of metal catalyst on semiconductors [11,12] and carbon

based (e.g. graphene and CNT) devices [13,14] have been studied to lower the operating temperature by reducing the energy required for gas adsorption [7]. Among them, Pd has been extensively used as a potential material for H<sub>2</sub> detection due to its large H<sub>2</sub> sticking coefficient, low activation barrier to H<sub>2</sub> adsorption, high diffusion rate, which further catalyzes dissociative adsorption and associative desorption for hydrogen [15,16].

The development of sensors based on field effect transistors (FET) compatible with VLSI fabrication draws special attention due to their chip scale miniaturization, low power consumption coupled with high performance metrics [17]. A vast amount of research has been conducted on the Pd-silicon dioxide (SiO<sub>2</sub>)-silicon structures with thick Pd films for H<sub>2</sub> sensing. Systematic experiments performed to study the H<sub>2</sub> adsorption at the Pd-SiO<sub>2</sub> interfaces shed light on the sensing mechanism [18–20]. Recently, silicon nanowire (Si NW) and Si FETs have shown excellent transduction and recognition of gas and bio chemical species due to their large surface to volume ratio and low power consumption. In addition, their compatibility with the state of the art complementary metal oxide (CMOS) technology allows scalability [21]. Several groups have reported considerable progress in H<sub>2</sub> sensing by fabricating Pd-NPs decorated Si NW FETs. In particular, Fahad *et al.* utilized a 3.5 nm thin Si channel on an insulator decorated with Ni-Pd NPs to detect H<sub>2</sub>; the detection limit was ~0.3% with saturation occurring above 0.5% giving a narrow sensing window [17]. This device exhibited a sensor response of ~600% when exposed to 1% H<sub>2</sub>. In another work, Ahn *et al.* have presented Pd NPs decorated Si NW FET (fabricated by top-down methods) with side gates for detection of H<sub>2</sub> [22]. The local side gates in this case allowed additional degrees of freedom to operate the device in the subthreshold regime contributing to enhanced sensitivity; they detected H<sub>2</sub> in the range of 0.1 to 1% with a sensor response of ~3500% at 1% H<sub>2</sub> exposure. In the subthreshold regime, the channel current carriers are almost depleted

and the conductance change due to gas adsorption gets drastically modified when operated in this regime. In spite of these advances, detecting lower concentrations of H<sub>2</sub> with high sensitivity, to allow time before it reaches the lower explosive limit of 4% and causes any explosion, still remains a significant challenge.

EFN sensors, a silicon-on-insulator (SOI) based multi-gate sensing technology have proven to be a promising platform for sensitive detection of various volatile organic compounds (VOCs) [23–25]. In these devices, the nanowire is electrostatically defined post fabrication by appropriate biasing of the junction and the back gates. In addition, their property of “electric-field controlled sensing” has been exploited to show selectivity for various VOCs through a single chemically unmodified sensing device [21]. This electric field controlled and enhanced sensing can be further improved by surface modification of the EFN sensor with metal NPs, which proves advantageous due to enhanced surface area and catalysis [17]. We present here ultra-sensitive H<sub>2</sub> detection based on Pd NPs decorated EFN sensor (Pd-EFN). We have studied the variation of parameters like tuning of gate voltages, impact of relative humidity and temperature on the sensor performances. The catalytic activity of the Pd NPs towards H<sub>2</sub> coupled with the channel narrowing effect of the EFN lead to H<sub>2</sub> sensor with excellent performances. This paves the way for scalable, low power, and inexpensive H<sub>2</sub> sensors. We also discuss the plausible gas sensing mechanism, which will help to design future H<sub>2</sub> sensors with superior performance.

## **2. Experimental section**

### *2.1. Device description and fabrication, electrical and sensing measurements*

The EFN sensor is a multiple gate accumulation type FET device (based on the four gate transistor introduced in the early 2000s) [26] that consists of a 150 nm thick SOI layer with a 6 nm

thick SiO<sub>2</sub> top dielectric exposed to the target molecules. The EFN derives its name from the concept that the nanowire is formed electrostatically by appropriate biasing of the surrounding gates: the junction gate bias  $V_{JG}$  applied to the two junction gates (p<sup>+</sup>-doped Si) on either side of the n-channel and the back gate bias  $V_{BG}$  applied to the p-type substrate beneath the buried oxide layer (BOX). Reverse biasing of the p-n junctions creates depletion regions, which confine the current conducting channel in the middle to a nanowire shape, the width and depth of which are suitably tuned by the applied biases. The EFN transistors were fabricated in a semiconductor foundry (*TowerJazz*, Migdal Haemek, Israel) using SOI technology in a CMOS process described in details in previous works [23–25]. The EFN device was mounted on a chip carrier via wire bonding for electrical measurements and H<sub>2</sub> sensing. The SiO<sub>2</sub> surface of EFN device was modified using Pd NPs (~1nm diameter) (which acts as a selective coating for H<sub>2</sub> gas) deposited using electron beam evaporation technique at a rate of 1Å/s; no annealing was performed post NPs deposition.

Electrical measurements were performed in a custom made sealed metallic gas chamber equipped with chip carrier holder, electrical feedthroughs and inlet and outlet for gases. Current-voltage ( $I$ - $V$ ) characteristics of the EFN device (both pre and post Pd NPs deposition) were measured using the Semiconductor Parameter Analyzer (SPA) B1500A, Agilent Technologies, Santa Clara which was connected to the device mounted in the chamber via electrical feedthroughs. The source and drain current and the voltages of the Pd-EFN device are  $I_{DS}$  and  $V_{DS}$  respectively, and the applied back gate and the junction gate voltages are  $V_{BG}$  and  $V_{JG}$ , respectively. The current-time ( $I$  vs  $t$ ) measurements for H<sub>2</sub> sensing were conducted using the same SPA.

The inlet to the gas chamber is connected to a customized gas delivery system consisting of dedicated gas lines and mass flow controllers (MFCs, Alicat Scientific Inc.) for target and carrier gases (Dry air/Nitrogen (N<sub>2</sub>)/Argon (Ar)). Desired concentration of H<sub>2</sub> gas was generated by controlling the ratio of the flow rates of the target and the carrier gases. The concentration of H<sub>2</sub> gas in the source cylinder was 4% with Ar as the residual gas. The experimental detection limit of the system was 0.02% H<sub>2</sub>. The total flow rate at any instant was kept constant at 1000 sccm to eliminate the effect of sensor response change due to change in pressure affected by different flow rates. In addition, for creating a humid atmosphere, a separate MFC was connected to the inlet of the bubbler system (water bath). Dry air was passed through this MFC to generate the moist air which was then directed to the chamber along with H<sub>2</sub>. We have controlled the flow rates of the dry air and humid air flowing through the water bath to control the relative humidity (RH). The RH in the chamber was monitored by a Thermohygrometer (DeltaOhm, Italy, HD 2101.1R). Specific flow rates (precalibrated using the hygrometer) allowed us to obtain a constant RH at the room temperature. The RH values were set at the room temperature of 20±2 °C (also measured by the thermohygrometer). For preconditioning and performing sensing experiments at different temperatures, the EFN device was heated with a pre-calibrated transistor based heater connected to the base of the chip carrier. The temperature of the heater was controlled by a temperature controller. A temperature sensor was also mounted to monitor the *in situ* temperature of the EFN device by an electronic feedback circuit.

## 2.2. Atomic Force Microscopy (AFM) and Kelvin Probe Force Microscopy (KPFM)

The KPFM and topography measurements were carried out using a commercial atomic force microscope (Dimension Edge, Bruker Inc. USA) inside a N<sub>2</sub> glovebox with platinum/iridium

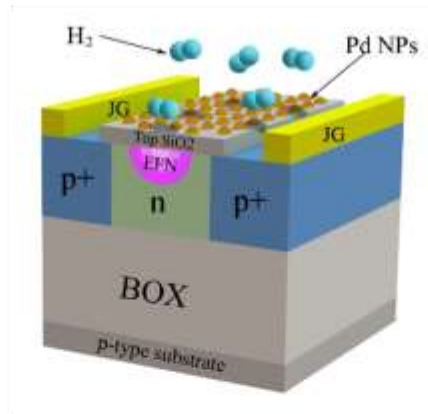
(95%/5%) coated cantilevers (PPP EFM, Nanosensors, Neuchatel, Switzerland). The contact potential difference (CPD) and topography were measured simultaneously using single scan amplitude modulation KPFM, and the effective (average) tip sample distance of  $\sim 10$  nm was maintained during scanning. In order to differentiate between the topography and the CPD signals, enhance the sensitivity, and maintain a minimum tip-sample distance, the ac electrostatic force component was generated at the second cantilever resonance,  $f_{\text{second}} \sim 450$  kHz, by applying an ac voltage of 500 mV.

### **3. Results and Discussion**

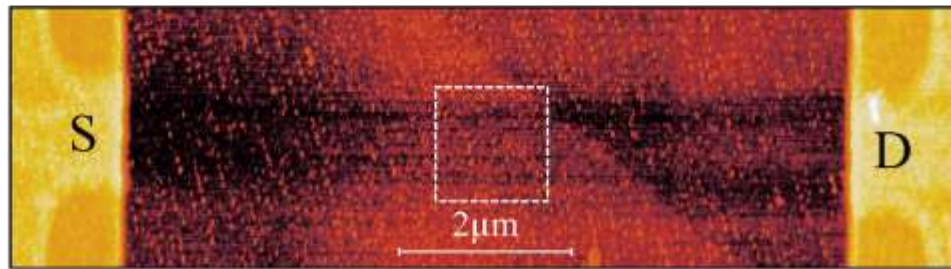
#### *3.1. AFM and KPFM characterization*

The schematic of Pd-EFN device is depicted in Fig. 1(a). Fig. 1(b) shows the AFM image of the surface of Pd-NPs modified EFN device. A uniform distribution of the Pd NPs was observed on the SiO<sub>2</sub> surface as indicated by the brighter yellow spots. The zoomed-in image in Fig. 1(c) (of the marked area in Fig. 1(b) shows magnified Pd NPs with average particle height varying between 1-2 nm, as indicated by the height profiles (of the NPs along the marked lines) in Fig. 1(d). A detailed statistical analysis of the distribution of the Pd NPs is provided in supplementary information (SI) through Fig. S1 and S2. The NPs formed a discontinuous layer on the top oxide (as evident from the AFM image, Fig. 1(c)) without short circuiting the junction gates, which would otherwise give rise to leakage currents in the device. The average distance between the NPs is  $\sim 75$  nm, which corresponds to an average density of NPs of  $\sim 4 \times 10^{10}$  cm<sup>-2</sup>. In this work, the surface coverage was controlled by the deposition time. However, we believe that, by optimizing the deposition process to further increase the Pd NPs coverage without increasing the leakage current, the sensitivity to H<sub>2</sub> can be substantially improved and this will be described in a future work.

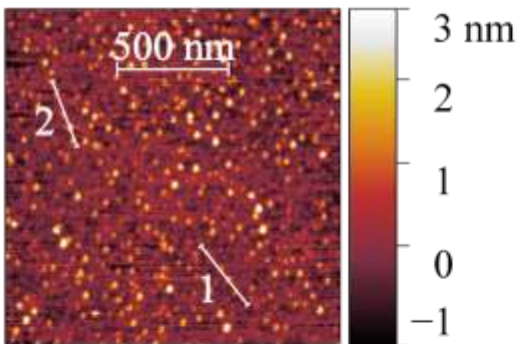
(a)



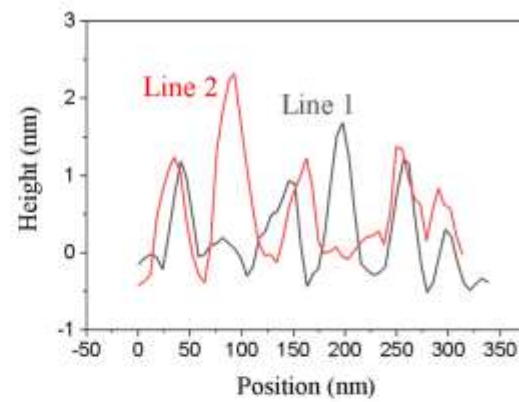
(b)



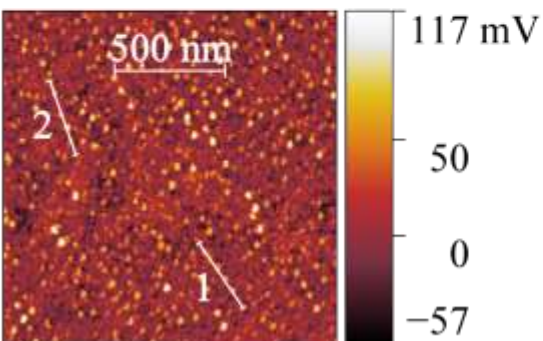
(c)



(d)



(e)



(f)

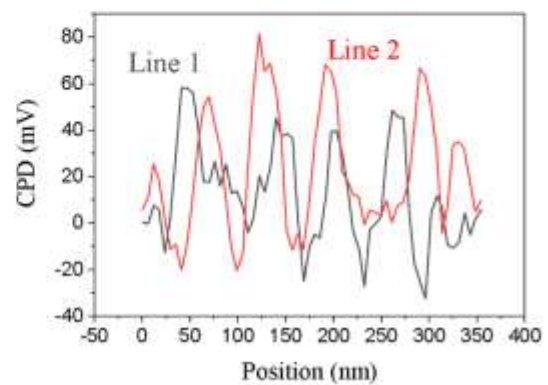


**Fig. 1.**

The KPFM image in Fig. 1(e) depicts the 2D potential image of the Pd NPs and the SiO<sub>2</sub> film. The CPD profiles in Fig. 1(f) of the NPs along the marked lines (in Fig. 1(e)) show a potential difference of around 40-80 mV between the Pd NPs and the SiO<sub>2</sub>. This potential difference is largely affected by the averaging effect of the KPFM probe (tip+cantilever), as described in details in our previous works [27,28]. Further, the interaction between the Pd NPs and the H<sub>2</sub> molecules, could possibly modulate the CPD profile which needs to be investigated.

### 3.2. Transfer characteristics of Pd NPs decorated EFN

Fig. 2(a) shows the  $I_{DS}-V_{BG}$  curve of the EFN transistor before and following surface modification with Pd NPs measured at  $V_{JG} = -2.5V$  and  $V_{DS} = 1V$ . A positive threshold voltage shift was observed following the Pd NPs decoration. The calculated electrostatic potential of the Pd-EFN channel following the surface modification with Pd NPs is shown in Fig. 2(b) in a cross sectional view. The simulations were carried out by *Sentaurus TCAD*, (Synopsys, Mountain View, USA) which solves the coupled continuity and the Poisson equations in 3D taking into account the EFN fabrication processes. With the increase in the number of NPs, the EFN channel is more depleted (indicated by the yellow regions) and the electron channel (the non-depleted region indicated by the white lines) becomes smaller. This is due to the work function difference across the Pd/SiO<sub>2</sub>/n-Si structure shown in Fig. 2(c) and (d). The work function of Pd is ~5.1 eV and that of n-Si is ~4.3 eV. This work function difference between n-Si and Pd creates an upward band bending at the SiO<sub>2</sub>/Si interface resulting in depletion and consequently contributing to a positive threshold shift of  $V_{BG}$  shown in Fig. 2(a). Such observations are consistent with prior reports of n-type semiconducting nanowire FETs [29–31].

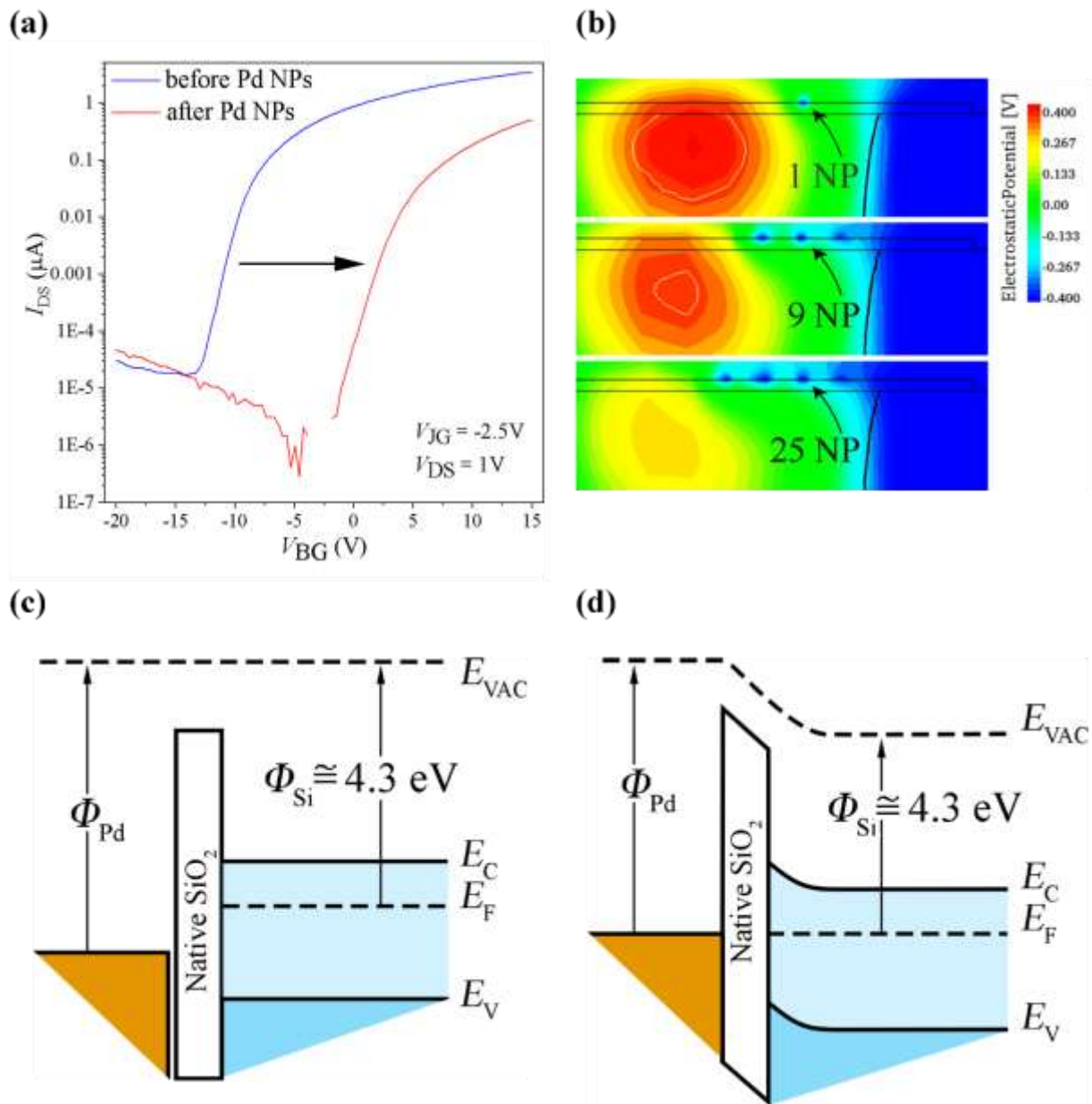


**Fig. 2.**

### 3.3. Transfer characteristics of Pd-EFN on $H_2$ sensing and recovery

To evaluate the H<sub>2</sub> sensing performances of the Pd-EFN sensor, it was exposed to different concentrations of H<sub>2</sub> gas in the range of 0.02 to 0.8% (200 to 8000 ppm). A concentration higher than 1% was avoided as it may lead to phase transformation of PdH<sub>x</sub> (from  $\alpha$  to  $\beta$  phase) and cause fast degradation of the device. A typical  $I_{DS}$ - $V_{BG}$  curve for 0.4 % H<sub>2</sub> exposure is shown in Fig. 3(a); the H<sub>2</sub> exposure leads to a negative back gate threshold voltage shift ( $\Delta V_{Th}(BG)$ ), which indicates a positive ‘gating’ effect of the hydrogen adsorption discussed in more details below. On turning off the H<sub>2</sub> flow, the Pd-EFN device recovers to its original  $I_{DS}$ - $V_{BG}$  curve (and threshold voltage) indicating complete H<sub>2</sub> desorption. Fig. 3(b) shows  $I_{DS}$ - $V_{BG}$  characteristics measured at different junction gates for 0.8 % H<sub>2</sub> exposure. These measurements were performed before and following the H<sub>2</sub> exposure of the device for 15 minutes (the device response typically saturated within 10 mins of exposure at each concentration). For a given H<sub>2</sub> concentration,  $\Delta V_{Th}(BG)$  decreases (increases in absolute values) with more negative  $V_{JG}$ . For a more negative  $V_{JG}$ , the initial (prior to H<sub>2</sub> exposure) size of the EFN channel is smaller, so the back gate voltage required for current onset,  $V_{Th}(BG)$ , is larger. Following exposure to H<sub>2</sub>, which induces a positive gating effect, the channel becomes less depleted, hence a smaller change in back gate voltage ( $\Delta V_{Th}(BG)$ ) will be required in order to turn the current on for a more positive  $V_{JG}$ . Consequently, at a specific  $V_{JG}$ ,  $\Delta V_{Th}(BG)$  decreases (increases in absolute value) with the H<sub>2</sub> concentration, as shown in Fig. 3(c) by a bar chart plot for a constant  $V_{DS}$  of 1V. With increasing H<sub>2</sub> concentration, the effect of the H<sub>2</sub> induced positive gating increases; consequently, a more negative back gate voltage is required to turn the current on from the initial conditions thus contributing to a more negative threshold voltage shift. A maximum shift of  $\sim$ -8V and  $\sim$ -19V was obtained at  $V_{JG} = -0.2V$  when the Pd-EFN was exposed to 0.02% and 0.8% H<sub>2</sub>, respectively. The change in the device work-function,  $\Delta WF$ , as a function of the change in  $V_{Th}(BG)$ , was estimated by solving the one dimensional Poisson’s

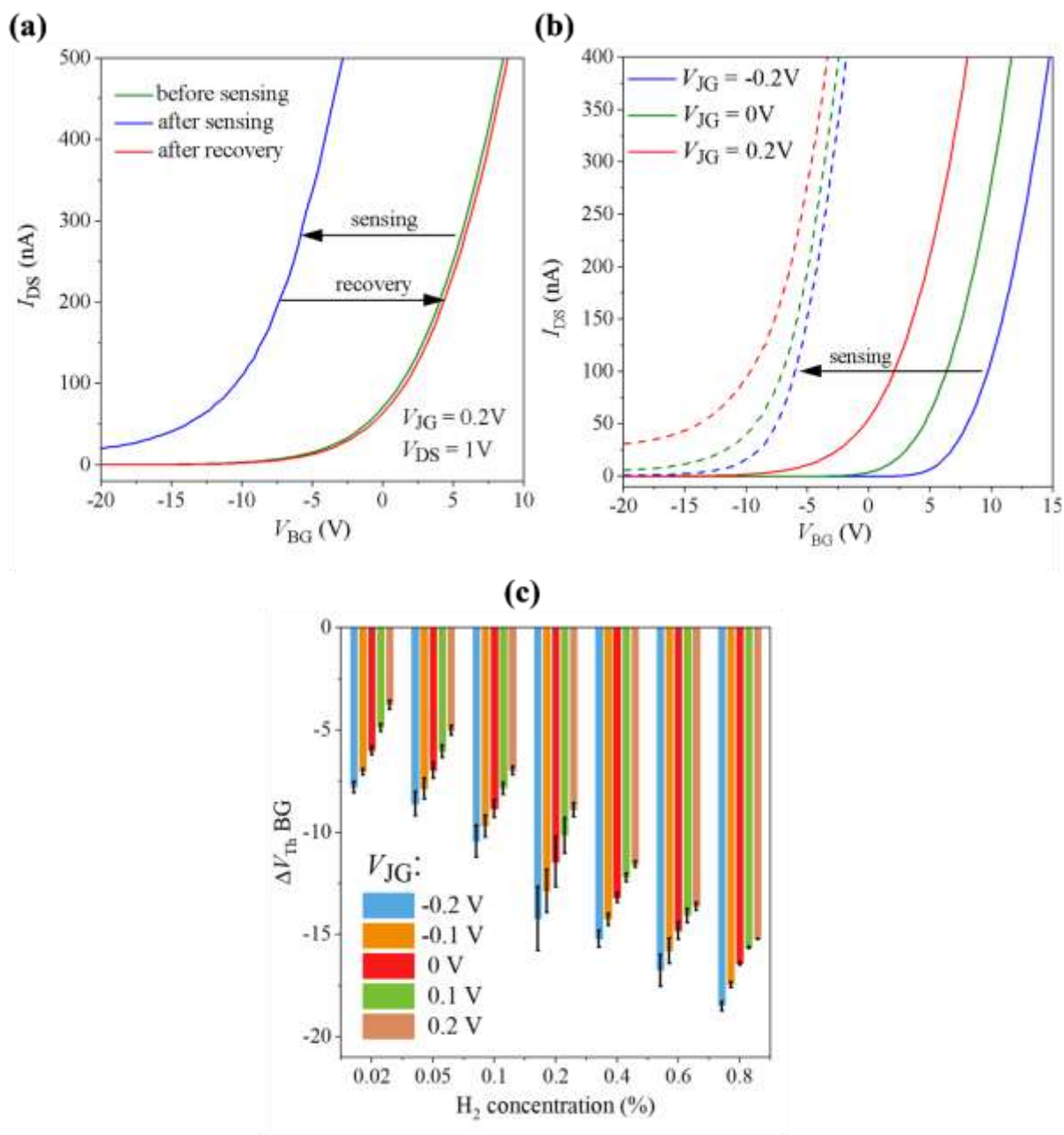


**Fig. 3.**

equation in the SOI region of the EFN device using appropriate boundary conditions (detailed calculation in SI). Based on this calculation, a back gate threshold voltage shift of 16V following exposure to 0.8% H<sub>2</sub> resulted in a work function change of 0.38 eV (details in SI).

### 3.4. H<sub>2</sub> Sensing characteristics of Pd-EFN

Fig. 4(a) shows the dynamic sensor response of the Pd-EFN device at room temperature (20±2 °C) to different concentrations of H<sub>2</sub> (0.02% to 0.8%) at different V<sub>JG</sub> with a constant V<sub>BG</sub> (0V) and V<sub>DS</sub> (1V). The back gate bias was kept at 0V in order to reveal the sole effect of the junction gate bias on the Pd-EFN sensing response. The sensor response, S, is defined in terms of the drain current as:

$$S (\%) = \frac{I_{\text{gas}} - I_0}{I_0} \times 100 \quad , \quad (1)$$

where  $I_0$  is the initial source-drain current in dry air prior to the H<sub>2</sub> exposure, and  $I_{\text{gas}}$  refers to the current following H<sub>2</sub> exposure. As expected, with increasing concentration of H<sub>2</sub> exposure, the sensor response increases. Also at a specific concentration, the sensor response increases with more negative V<sub>JG</sub>. This is consistent with the above observation, that  $\Delta V_{\text{Th}}$  (BG) decreases with more negatively biased junction gate at a fixed V<sub>DS</sub>. For V<sub>JG</sub> = -0.2V, the sensor response is ~9000% at 0.8% H<sub>2</sub> exposure. At this V<sub>JG</sub> and V<sub>DS</sub>, the initial I<sub>DS</sub> was ~ 1nA thus contributing to a minimum power consumption of 1nW. The sensor response is greatly enhanced by applying a more negative back gate voltage, which decreases the EFN channel size and the initial I<sub>DS</sub> to ~ 20 pA. A smaller channel current (implying almost a fully depleted channel) increases the sensor response to an unprecedented value of ~2 x 10<sup>6</sup> % at the same H<sub>2</sub> concentration (0.8%), as shown in Fig. 4(b). This increased sensitivity is due to the smaller EFN channel size under a more negative V<sub>BG</sub>; a smaller channel leads to larger relative current change (response) following H<sub>2</sub> adsorption.

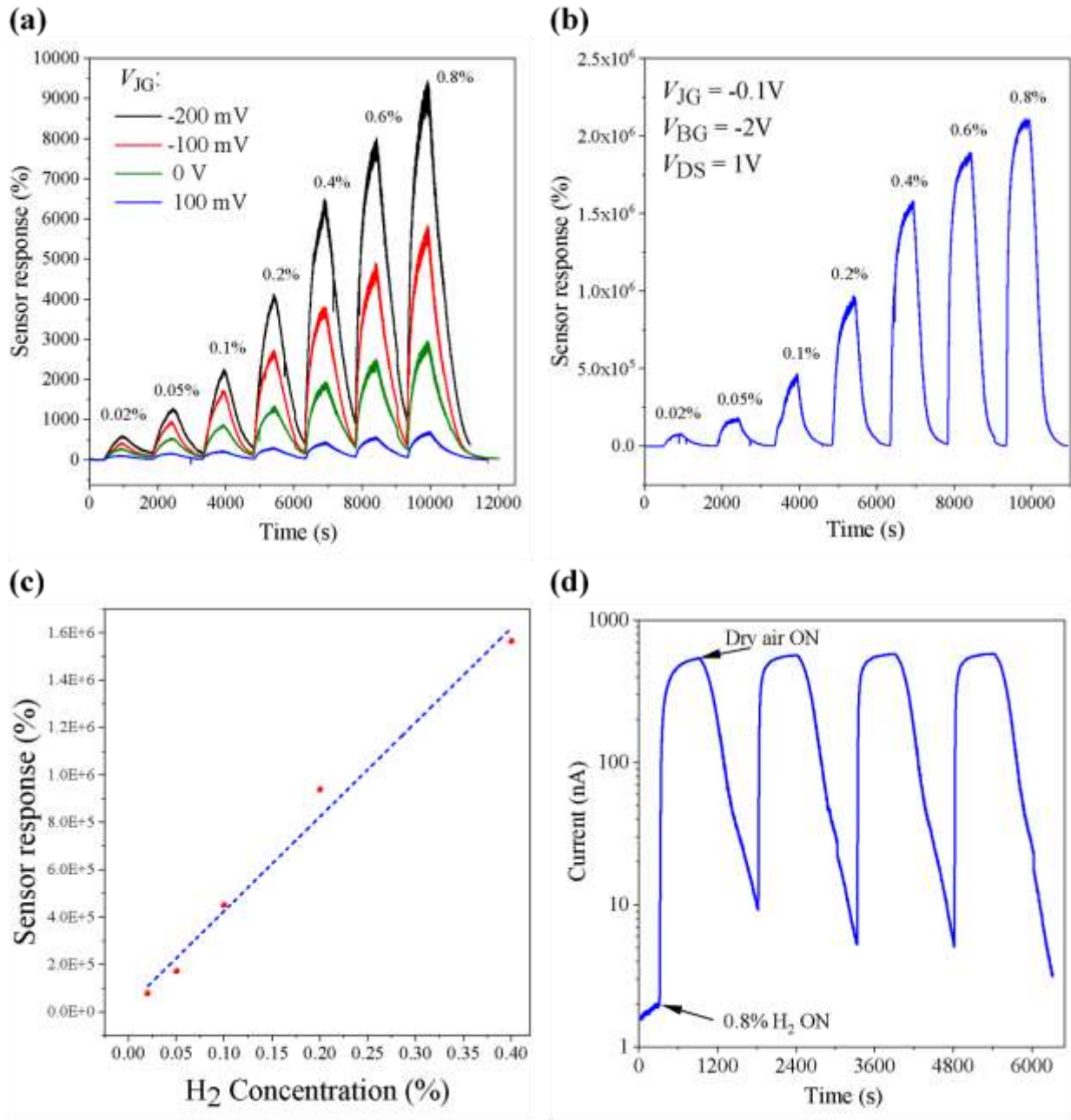


**Fig. 4.**

The power consumption in this case at the starting conditions was in pW. Even at maximum current flow ( $\sim 436$  nA) in the channel at 0.8% H<sub>2</sub> exposure, the power consumption was  $\sim 436$  nW. This

ultra-low power consumption along with the ultra-high sensitivity and the VLSI compatibility of the EFN device makes the Pd-EFN sensor very attractive for practical applications.

The sensitivity of the Pd-EFN to H<sub>2</sub> was found to be  $398 \pm 27\%$  ppm<sup>-1</sup> by a linear fitting of the sensor response as a function of concentration in the range of 0.02 to 0.4% (Fig. 4(c)). The detection limit of the Pd-EFN sensor was calculated to be ~42 ppb (details in SI). In order to emphasize the advantage of the Pd NPs surface modification relative to that of bare EFN, the sensor response of the latter towards H<sub>2</sub> is depicted in Fig. S3 in SI. The figure indicates that the untreated EFN shows merely 25.4% response to 2% H<sub>2</sub> exposure at appropriate biasing conditions in the subthreshold region. In addition, the current of the bare EFN channel decreases on H<sub>2</sub> gas exposure and does not recover on H<sub>2</sub> withdrawal. The Pd-EFN device also exhibited highly stable sensor response for many cycles, as depicted in Fig. 4(d) for four cycles reaching the same maximum current in each cycle on 0.8% H<sub>2</sub> exposure.

### *3.5. Effect of temperature on the H<sub>2</sub> Sensing characteristics of Pd-EFN*

The effect of temperature was also studied on the sensing performances of Pd-EFN. Fig. 5(a) depicts the time dependent EFN sensor response curves at various concentrations of H<sub>2</sub> measured at six different temperatures. These graphs were obtained at the biasing conditions of  $V_{BG}=0V$ ,  $V_{IG}=-0.1V$  and  $V_{DS}=1V$ , which do not give optimal response. The sensor responses at each H<sub>2</sub> concentration are further plotted as a function of temperature in Fig. 5(b). It is observed that the maximum sensor response for all concentrations is at around 45 °C. At this temperature, the Pd-EFN exhibits a sensor response of  $1.7 \times 10^4\%$  for 0.8% H<sub>2</sub> exposure. This is a 1.89 fold increase relative to the sensor response at room temperature under the same biasing conditions. The initial increase in sensor response with increased temperature can be attributed to the lower activation

energy for H<sub>2</sub> adsorption. However, for temperatures higher than 45 °C, the sensor response at all the measured H<sub>2</sub> concentrations decreases. This is plausible due to the decrease in sticking coefficient of H<sub>2</sub> and decrease in H<sub>2</sub> solubility in Pd with increasing temperature, as was reported for other Pd based H<sub>2</sub> sensors. The Pd-EFN device was operated in the subthreshold regime for obtaining optimal sensing response. It has recently been shown by our group [32] that the current in the EFN channel increases with temperature when operated in the subthreshold regime due to increase in carrier concentration. This larger EFN channel current at high temperatures may also contribute to decreased relative sensor response.

The sensor response time is commonly defined as the time by which the sensor signal (current) changes from 0 to 90% of the total response following gas exposure; the recovery time is defined in a similar manner as the time by which the sensor signal changes from its maximum to 10 % after stopping the gas flow. The Pd-EFN sensor response and recovery times are plotted at two different temperatures for different concentrations of H<sub>2</sub> in Fig. 5(c) and (d), respectively. The typical response time of the Pd-EFN varied from ~78 s to ~504 s for the entire range of exposure. The overall dependence is weak, but it is observed that with increase in concentration, the response time decreases, the effect being more pronounced at higher temperatures. Also, at a given concentration, the response time decreases with increase in temperature (data not shown). A shorter response time is obtained due to faster diffusion and dissociation of H<sub>2</sub> at higher temperatures. The Pd-EFN device exhibited the best sensor response time of ~78 s at 56 °C at 0.8% H<sub>2</sub> exposure (Fig. 5(c)) while it was ~390 s at room temperature. These values are comparable to some of the literature reported data, as shown below in Table 1. The typical recovery

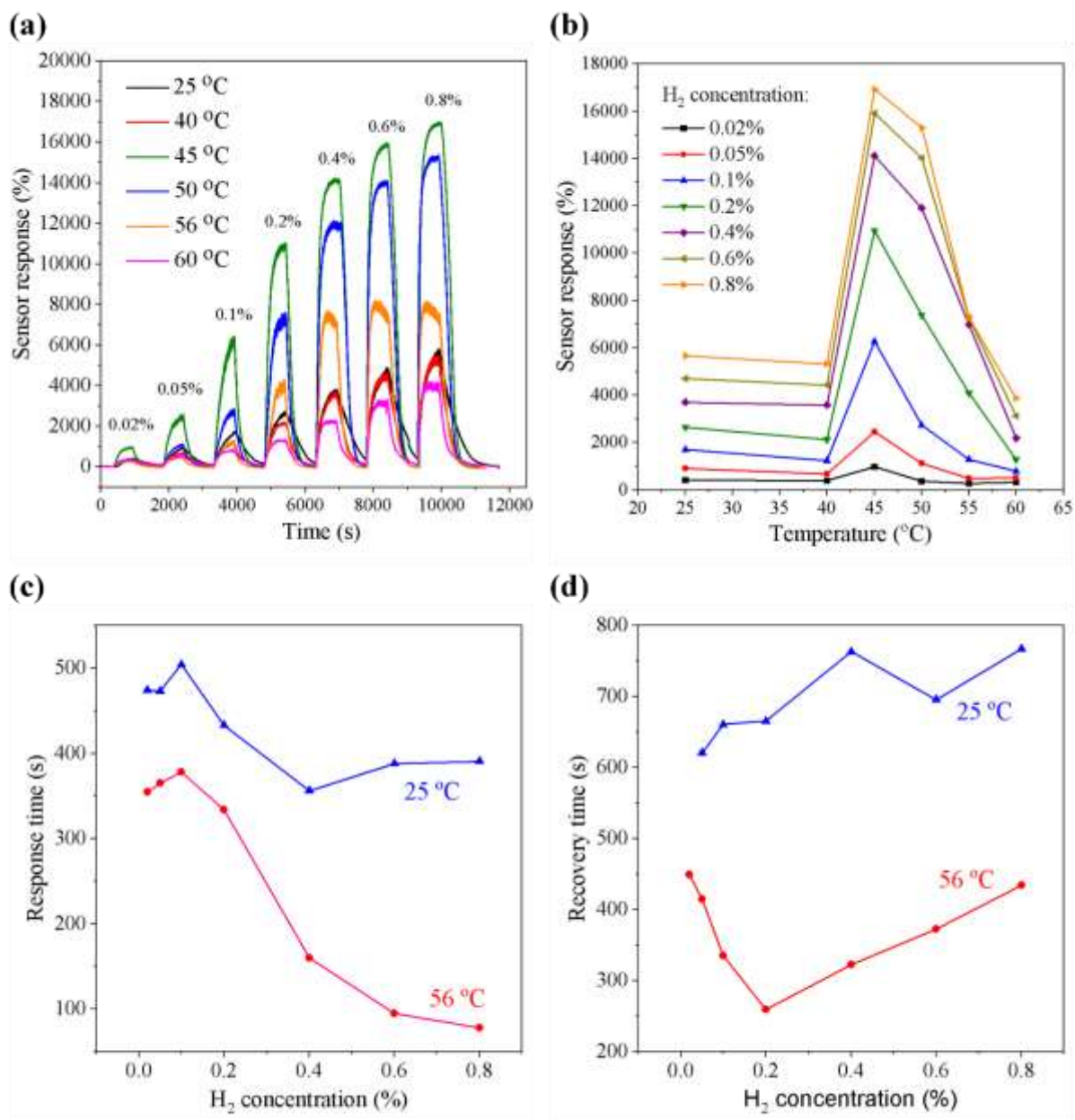


**Fig. 5.**

time of the sensor varied from ~260 to ~767 s for the entire range of H<sub>2</sub> exposure; the recovery time also improved with temperature till 56 °C (Fig. 5(d)). The recovery time of the sensor was ~434 s at 56 °C and ~767 s at room temperature for 0.8% H<sub>2</sub> exposure. We should note that the

response time evaluation of the sensor is strongly affected by the geometry of the sensing chamber. The response and recovery times will be much shorter by using a chamber with optimal fluid dynamics design.

### *3.6. Effect of relative humidity on the H<sub>2</sub> Sensing characteristics of Pd-EFN*

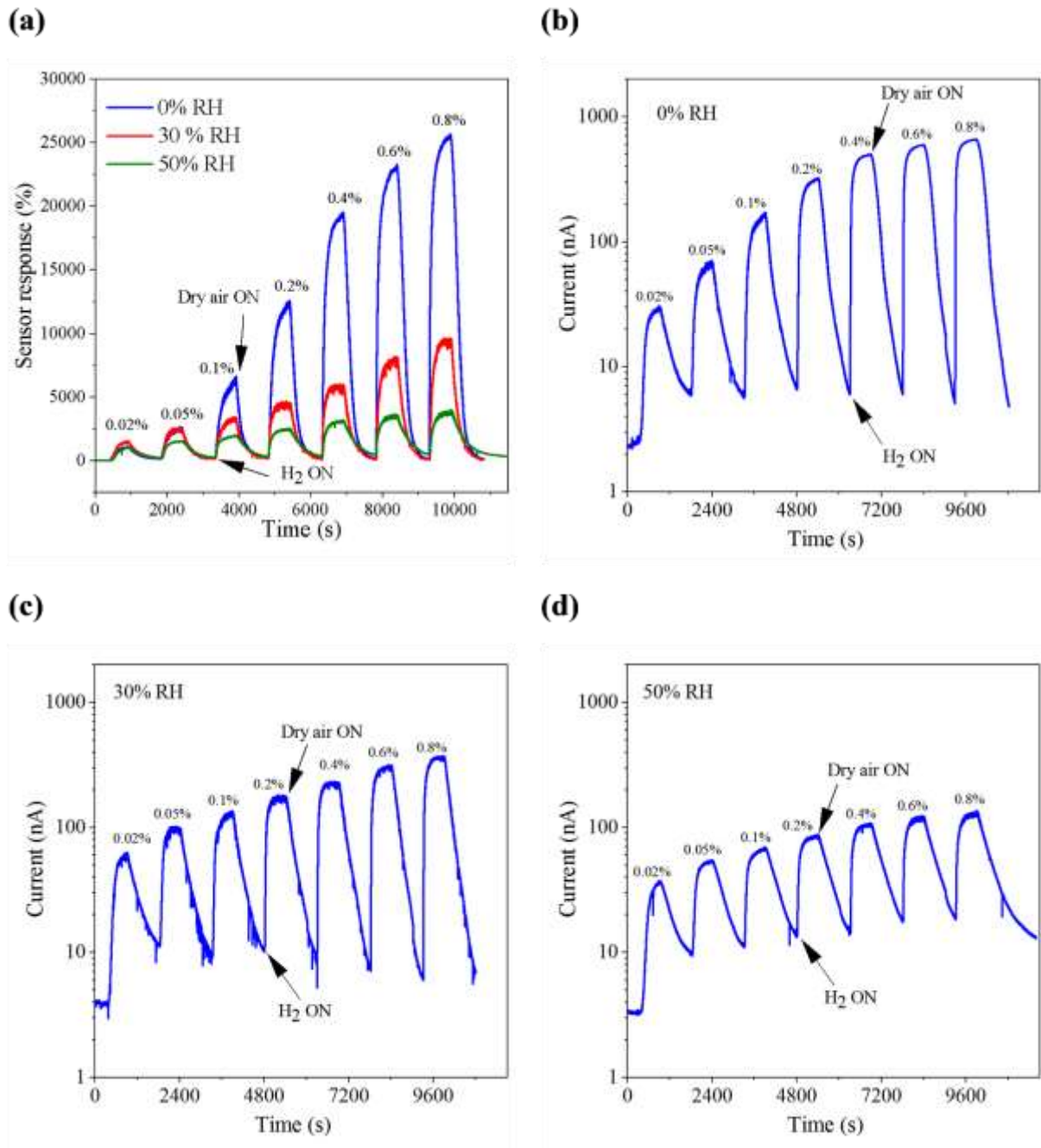


**Fig. 6.**

A practical hydrogen sensor should be able to function well under humid conditions. The effect of humidity (at room temperature of  $20 \pm 2$  °C) on the sensing characteristics of Pd-EFN is depicted

in Fig. 6(a) for 30% (red) and 50% (blue) RH, keeping the same bias conditions as at 0% RH. It is observed that with increasing humidity the sensor response decreases at all H<sub>2</sub> concentrations, although it is more pronounced at higher concentrations. A similar trend was observed under other biasing conditions. The decrease in sensitivity might be explained by the competition for adsorption sites on the surface of Pd NPs between water and H<sub>2</sub> molecules. At higher humidity, more adsorbed water molecules decrease the H<sub>2</sub> adsorption due to less available adsorption sites and hence the sensor response decreases. At lower H<sub>2</sub> concentrations (0.02 and 0.05%), the decrease in sensor response under higher humidity is very small (as can be observed in Fig. 6a) due to a larger number of available adsorption sites for H<sub>2</sub>. Nonetheless, the sensor response even under 50% RH (~2500% at 0.8% H<sub>2</sub> exposure) is comparable to the sensitivity reported by others for dry conditions as can be observed in Table 1. The response transients are also plotted by using actual current values (Fig. 6(b-d)) for clarity to the readers on the effect of humidity on the base sensor current. The base current values of the Pd-EFN at 0%, 30% and 50 % RH at the given biasing conditions was between 2-4 nA.

Table 1 compares the sensor performance metrics of the present Pd-EFN sensor with the state-of-the-art reported H<sub>2</sub> sensors based on Pd nanostructures, Pd NPs decorated Si, graphene, InGaP, and metal oxides (both in resistor and FET configurations). It shows that the Pd-EFN sensor is one of the potential candidates for practical H<sub>2</sub> sensing in terms of sensor response, dynamic range and power consumption. This is in addition to its two main advantages of VLSI compatibility and intrinsic selectivity.

**Table 1.** Comparison of the sensor performance metrics of our Pd-EFN sensor with the recently reported H<sub>2</sub> sensors at room temperature based on Pd nanostructures and Pd NPs decorated various sensing materials.

	Sensor specifications	Response [%]		Dyanamic range [%]	Response time [s] [H <sub>2</sub> ] ~1%	Recovery time (s) [H <sub>2</sub> ] ~1%	power consumption	Ref
		[H <sub>2</sub> ]~ 0.1%	[H <sub>2</sub> ]~ 1%					
Resistor	Pd NP @ rough Si	294	446	50 ppm-0.8%	32	110	1.62 μW	[33]
	Pd NP @ vertically aligned Si NWs	320	1700	5 ppm-1%	-	-	-	[34]
	Pd NP @ Si nanomesh	10	27	50 ppm-0.8%	5	13	400 μW	[35]
	Pd NP @ Si NW	0.80	-	0.1-1%	5	13	1.04 μW	[36]
	Pd@graphene	-	5.88	1-4%	180	540	0.98 mW (external light)	[37]
	Pd Nanotubes	1000	3754	0.01-1%	~210	-	-	[38]
FET	Ni and Pd NP @Si thin flim	90	550	0.3-2%	~30	~80 (t50)	0.34 nW	[17]
	Pd NP @ Si NW	625	3400	0.1-1%	7	-	-	[22]
	Pd-based SiO <sub>2</sub> InGaP/InGaAs	-	1.674 x 10 <sup>5</sup>	0.1-1%	-	-	-	[39]
	<i>This work (Pd-EFN)</i>	<i>~4 x 10<sup>5</sup></i>	<i>2x10<sup>6</sup></i>	<i>0.02-1%</i>	<i>78 [0.8% H<sub>2</sub>] at 56 °C</i>	<i>434 [0.8% H<sub>2</sub>] at 56 °C</i>	<i>few pW and 436 nW ( at max current consumption)</i>	

### 3.7. Gas sensing mechanism

The origin of H<sub>2</sub> sensitivity in Pd-based sensors has been discussed extensively, and various models have been reported in the literature (see e.g. the recent perspective [40]). The increase in current in Pd-Si-FET-based sensors following H<sub>2</sub> adsorption is commonly attributed to changes in band bending at the SiO<sub>2</sub>/Si interface of the transistor channel. One of the widely accepted models by Lundstrom *et al.* [41] is based on the fact that Pd nanoparticles catalyze the dissociation of H<sub>2</sub> molecules into atoms on the Pd surface. It suggests that the H atoms then diffuse to the Pd/SiO<sub>2</sub>

interface and create an “interfacial polarization layer”, which behaves like an ideal dipole layer with the hydrogen very close to the metal surface [42]. This induced dipole layer changes the Pd surface work function and consequently the channel band bending. This band bending changes the transistor threshold voltage, or the C-V characteristics in the case of capacitor based sensors. Induced dipoles due to H adsorption on the Pd surface will hardly affect the band bending due to screening by the underlying metallic NP. Also, H<sub>2</sub> adsorption in the form of PdH<sub>x</sub> (alpha phase) does not contribute significantly to work function change of the Pd due to the very small H concentration. The dipole layer is therefore most likely formed at the Pd/SiO<sub>2</sub> interface. Density Functional Theory (DFT) calculations of H at Pd/SiO<sub>2</sub> interface [43] have concluded that even high H concentration does not induce a potential change required for changes in C-V characteristics or threshold voltage. These calculations were carried out using the Generalized Gradient Approximation (GGA) of DFT and did not take into account that the SiO<sub>2</sub> surface is hydroxylated in humid air. More recent calculations suggest that there is charge transfer and dipole formation upon adsorption of hydrogen on Pd surface [44]. However, more detailed theoretical studies of the interface dipole layer formation at Pd/SiO<sub>2</sub> interfaces are still missing. Below we attempt to rationalize our results in a simple model based on the existing literature data (see also Fig. 7).

Most of the reports based on Lundstrom’s model [18] also mention that increased hydrogen sensitivity is observed under N<sub>2</sub> and Ar environments. However, control H<sub>2</sub> sensing experiments in N<sub>2</sub> and Ar environments with our Pd-EFN device have shown that the oxygen presence in the dry air environment, in which our measurements are conducted, facilitate H<sub>2</sub> adsorption and desorption. In particular, as shown in Fig. S4 in SI, the sensor responses to 0.4 and 0.8% H<sub>2</sub> are much weaker in N<sub>2</sub>. It has been observed previously that N<sub>2</sub> may be chemisorbed on air exposed

Pd surface thus interfering with H<sub>2</sub> adsorption [45] which possibly explains the reason of insignificant response with our Pd-EFN sensor in N<sub>2</sub> ambience. Similarly, with Ar as carrier gas, the sensor response of a representative Pd-EFN sample is high only for the first cycle and does not show complete recovery (Fig. S5 in SI). However, dry air facilitates complete recovery. Even though we observe substantial sensor response in Ar ambience, the use of Ar ambience is not practical and incomplete recovery at room temperature proves to be a bottleneck for practical sensing purposes.

The interaction of oxygen with Pd has been studied extensively (see e.g. [46] and references therein). The effect of oxygen depends on the oxygen pressure and exposed Pd surface and may lead to formation of PdO crystallites at high coverage. Schematic model of different stages of the interaction of H<sub>2</sub> with Pd-decorated EFN surface is shown in Fig. 7. We assume that oxygen can be adsorbed in the form of anions (O<sub>2</sub><sup>-</sup>, O<sup>-</sup> and O<sup>2-</sup>) on the Pd surface, [47] which modulates the work function of the metal, as depicted in Fig. 7(a). In fact, a negative charge buildup due to oxygen anions on the Pd surface can result in increase in the work function of Pd [47]. This can explain the depletion of electrons at the Si/SiO<sub>2</sub> interface and a positive threshold voltage shift due to dry air exposure of the Pd-EFN device from N<sub>2</sub> ambience (Fig. S6 in SI).

On initial H<sub>2</sub> exposure, removal of oxygen anions take place due to formation of water molecules which

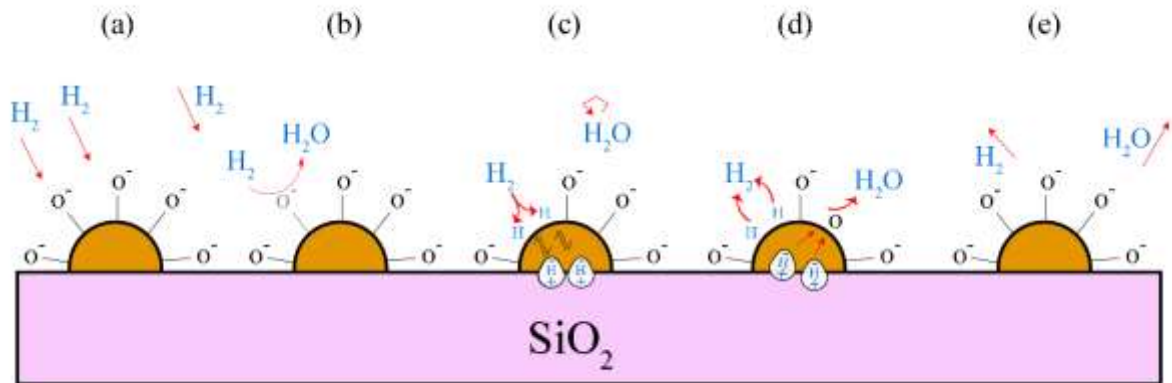


**Fig. 7.**

decrease the Pd work function (Fig. 7(b)) [48]. This oxygen removal creates more available sites for additional hydrogen adsorption; consequently more hydrogen atoms can reach the Pd/SiO<sub>2</sub> interface creating dipoles and further decreasing the work function, as illustrated in Fig. 7(c). A detailed study [49] has concluded that hydrogen dissociatively adsorbs below 100 K on the PdO (101) surface and that most of the dissociated hydrogen reacts with the surface oxygen to produce water desorbing at about 350 K. We note that this water desorption temperature agrees well with the temperature corresponding to the highest sensor sensitivity observed in this work. This desorption phenomenon is illustrated in Fig. 7(d). On removal of H<sub>2</sub>, initial conditions are restored as depicted in Fig. 7(e) allowing the sensor to recover to its baseline. This cumulative decrease in work function, as explained above, induces electron accumulation in the conducting channel depicted in Fig. 8, and causes a negative shift in the threshold voltage shown in Fig. 3(a).

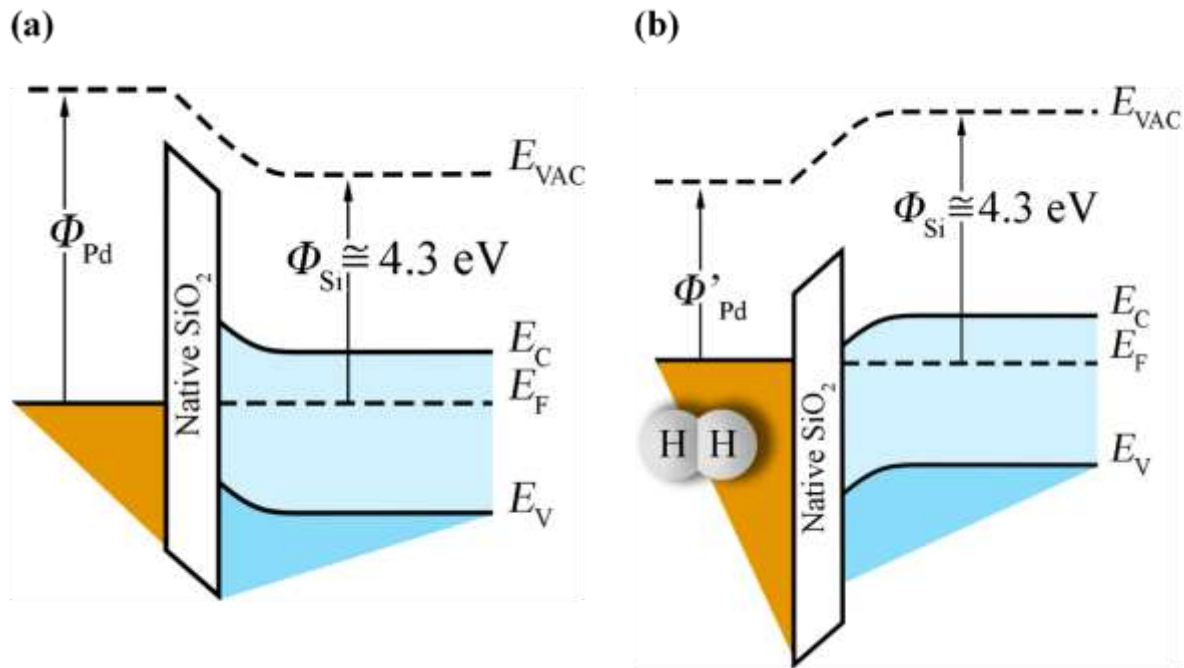


**Fig. 8.**

It has been shown experimentally that the H atoms at the interface and the surface are always in equilibrium due to their high diffusion coefficient [18]. Hence when the H<sub>2</sub> flow stops, the H atoms from the interface reach the surface and react with oxygen present in dry air for efficient water desorption from the Pd surface, which is unlike the case when the surface is covered by N<sub>2</sub>/ Ar molecules.

It is instructive to understand the mechanism responsible for the superior response of the Pd-EFN sensor relative to similar devices (see Table 1). One plausible explanation is the ability to tune electrostatically the ‘nanowire like’ channel to the size and location which will result in the highest sensitivity. The optimal biasing conditions might differ from analyte to analyte, but they can be optimized post fabrication. In all FET-based devices the working point can be adjusted to the sub-threshold regime to maximize sensitivity. However, in the EFN device the channel shape

can be tuned at the optimal working point to maximize sensitivity. In addition, the effect of the surface fringing electric field at the sensor surface is enhanced from  $1 \times 10^5$  to  $1 \times 10^6$  V/cm at the vicinity of the Pd nano-size particles. Study is in progress to find if this large electric field also contributes to the enhanced sensor response.

## 4. Conclusions

In summary, we have developed an ultra-sensitive, robust, ultra-low powered H<sub>2</sub> sensor based on Pd NPs decorated EFN sensor. Appropriate tuning of the EFN gate biases resulted in an unprecedented sensor response of  $2 \times 10^6$  % to 0.8% H<sub>2</sub> and a sensitivity of  $\sim 400\%$  ppm<sup>-1</sup> which outperforms, to the best of our knowledge, most of the state of the art resistive and FET based H<sub>2</sub> sensors. The sensor response and recovery kinetics are further improved at a temperature around 45°C. It was found that the presence of oxygen influences the sensor response and recovery kinetics, while increased humidity degrades the performance. In conclusion, deposition of Pd NPs in conjunction with the tunable channel of the EFN platform, pave the way for the development of high performance H<sub>2</sub> sensor in order to meet the growing demands to support the safe usage of H<sub>2</sub> as the alternative source of clean and renewable energy.

**APPENDIX A.** *Supplementary data:* Statistical analysis of distribution of Pd-NPs on EFN surface; Calculation of workfunction change corresponding to threshold voltage change; Response of bare EFN to H<sub>2</sub>; Calculation of theoretical detection limit of Pd-EFN sensor; Influence of N<sub>2</sub> and Ar ambient on H<sub>2</sub> sensing characteristics of Pd-EFN.

## Acknowledgements

A.M would like to acknowledge the support of the Tel Aviv University Center for Nanoscience and Nanotechnology. A.M. would also like to acknowledge scientific inputs from Dr. Nandhini

Swaminathan and Dr. Anjan Bhukta. <sup>¶</sup>M. Gnaim and I. S. Tov have contributed equally to this work.

## References:

- [1] A. Hussain, S.M. Arif, M. Aslam, Emerging renewable and sustainable energy technologies: State of the art, *Renew. Sustain. Energy Rev.* 71 (2017) 12–28. doi:10.1016/j.rser.2016.12.033.
- [2] A. Mirzaei, H.R. Yousefi, F. Falsafi, M. Bonyani, J.H. Lee, J.H. Kim, H.W. Kim, S.S. Kim, An overview on how Pd on resistive-based nanomaterial gas sensors can enhance response toward hydrogen gas, *Int. J. Hydrogen Energy.* 44 (2019) 20552–20571. doi:10.1016/j.ijhydene.2019.05.180.
- [3] P.E. Dodds, I. Staffell, A.D. Hawkes, F. Li, P. Grünewald, W. McDowall, P. Ekins, Hydrogen and fuel cell technologies for heating: A review, *Int. J. Hydrogen Energy.* 40 (2015) 2065–2083. doi:10.1016/j.ijhydene.2014.11.059.
- [4] M.Z. Jacobson, W.G. Colella, D.M. Golden, Atmospheric science: Cleaning the air and improving health with hydrogen fuel-cell vehicles, *Science* (80-. ). 308 (2005) 1901–1905. doi:10.1126/science.1109157.
- [5] S.Y. Cho, H. Ahn, K. Park, J. Choi, H. Kang, H.T. Jung, Ultrasmall Grained Pd Nanopattern H<sub>2</sub> Sensor, *ACS Sensors.* 3 (2018) 1876–1883. doi:10.1021/acssensors.8b00834.
- [6] H. Gu, Z. Wang, Y. Hu, Hydrogen Gas Sensors Based on Semiconductor Oxide Nanostructures, *Sensors.* 12 (2012) 5517–5550. doi:10.3390/s120505517.
- [7] L. Du, M. Yuan, H. Wei, X. Xing, D. Feng, Y. Liao, H. Chen, D. Yang, Interconnected Pd Nanoparticles Supported on Zeolite-AFI for Hydrogen Detection under Ultralow Temperature, *ACS Appl. Mater. Interfaces.* 11 (2019) 36847–36853. doi:10.1021/acscami.9b12272.
- [8] S.J. Choi, S. Chattopadhyay, J.J. Kim, S.J. Kim, H.L. Tuller, G.C. Rutledge, I.D. Kim, Coaxial electrospinning of WO<sub>3</sub> nanotubes functionalized with bio-inspired Pd catalysts and their superior hydrogen sensing performance, *Nanoscale.* 8 (2016) 9159–9166. doi:10.1039/c5nr06611e.
- [9] R. Deivasegamani, G. Karunanidhi, C. Santhosh, T. Gopal, D. Saravana achari, A. Neogi, R. Nivetha, N. Pradeep, U. Venkatraman, A. Bhatnagar, S.K. Jeong, A.N. Grace, Chemoresistive sensor for hydrogen using thin films of tin dioxide doped with cerium and palladium, *Microchim. Acta.* 184 (2017) 4765–4773. doi:10.1007/s00604-017-2514-7.
- [10] K. Nguyen, C.M. Hung, T.M. Ngoc, D.T. Thanh Le, D.H. Nguyen, D. Nguyen Van, H.

- Nguyen Van, Low-temperature prototype hydrogen sensors using Pd-decorated SnO<sub>2</sub> nanowires for exhaled breath applications, *Sensors Actuators, B Chem.* 253 (2017) 156–163. doi:10.1016/j.snb.2017.06.141.
- [11] J. Zhang, X. Liu, G. Neri, N. Pinna, Nanostructured Materials for Room-Temperature Gas Sensors, *Adv. Mater.* 28 (2016) 795–831. doi:10.1002/adma.201503825.
- [12] P.A. Russo, N. Donato, S. Gianluca Leonardi, S. Baek, D.E. Conte, G. Neri, N. Pinna, P.A. Russo, D.E. Conte, N. Pinna, N. Donato, S.G. Leonardi, G. Neri, S. Baek, Room-Temperature Hydrogen Sensing with Heteronanostructures Based on Reduced Graphene Oxide and Tin Oxide\*\*, *Angew. Chem. Int. Ed.* 51 (2012) 11053–11057. doi:10.1002/anie.201204373.
- [13] V.S. Bhati, S. Ranwa, S. Rajamani, K. Kumari, R. Raliya, P. Biswas, M. Kumar, Improved Sensitivity with Low Limit of Detection of a Hydrogen Gas Sensor Based on rGO-Loaded Ni-Doped ZnO Nanostructures, *ACS Appl. Mater. Interfaces.* 10 (2018) 11116–11124. doi:10.1021/acsami.7b17877.
- [14] G. Lu, L.E. Ocola, J. Chen, Room-Temperature Gas Sensing Based on Electron Transfer between Discrete Tin Oxide Nanocrystals and Multiwalled Carbon Nanotubes, *Adv. Mater.* 21 (2009) 2487–2491. doi:10.1002/adma.200803536.
- [15] F.A.A. Nugroho, I. Darmadi, L. Cusinato, A. Susarrey-Arce, H. Schreuders, L.J. Bannenberg, A.B. da Silva Fanta, S. Kadkhodazadeh, J.B. Wagner, T.J. Antosiewicz, A. Hellman, V.P. Zhdanov, B. Dam, C. Langhammer, Metal–polymer hybrid nanomaterials for plasmonic ultrafast hydrogen detection, *Nat. Mater.* 18 (2019) 489–495. doi:10.1038/s41563-019-0325-4.
- [16] M. Khanuja, S. Kala, B.R. Mehta, F.E. Kruis, Concentration-specific hydrogen sensing behavior in monosized Pd nanoparticle layers, *Nanotechnology.* 20 (2009). doi:10.1088/0957-4484/20/1/015502.
- [17] H.M. Fahad, H. Shiraki, M. Amani, C. Zhang, V.S. Hebbbar, W. Gao, H. Ota, M. Hettick, D. Kiriya, Y.Z. Chen, Y.L. Chueh, A. Javey, Room temperature multiplexed gas sensing using chemical-sensitive 3.5-nm-thin silicon transistors, *Sci. Adv.* 3 (2017) e1602557. doi:10.1126/sciadv.1602557.
- [18] L.G. Ekedahl, M. Eriksson, I. Lundström, Hydrogen Sensing Mechanisms of Metal-Insulator Interfaces, *Acc. Chem. Res.* 31 (1998) 249–256. doi:10.1021/ar970068s.
- [19] I. Lundström, Hydrogen sensitive mos-structures. Part 1: Principles and applications, *Sensors and Actuators.* 1 (1981) 403–426. doi:10.1016/0250-6874(81)80018-2.
- [20] M. Eriksson, L.G. Ekedahl, Hydrogen adsorption states at the Pd/SiO<sub>2</sub> interface and simulation of the response of a Pd metal-oxide-semiconductor hydrogen sensor, *J. Appl. Phys.* 83 (1998) 3947–3951. doi:10.1063/1.367150.
- [21] N. Mahapatra, A. Ben-Cohen, Y. Vaknin, A. Henning, J. Hayon, K. Shimanovich, H. Greenspan, Y. Rosenwaks, Electrostatic Selectivity of Volatile Organic Compounds Using Electrostatically Formed Nanowire Sensor, *ACS Sensors.* 3 (2018) 709–715.

- doi:10.1021/acssensors.8b00044.
- [22] J.-H. Ahn, J. Yun, Y.-K. Choi, I. Park, Palladium nanoparticle decorated silicon nanowire field-effect transistor with side-gates for hydrogen gas detection, (n.d.).  
doi:10.1063/1.4861228.
- [23] N. Swaminathan, A. Henning, Y. Vaknin, K. Shimanovich, A. Godkin, G. Shalev, Y. Rosenwaks, Dynamic Range Enhancement Using the Electrostatically Formed Nanowire Sensor, *ACS Sensors*. 1 (2016) 688–695. doi:10.1021/acssensors.6b00096.
- [24] N. Swaminathan, A. Henning, T. Jurca, J. Hayon, G. Shalev, Y. Rosenwaks, Effect of varying chain length of n-alcohols and n-alkanes detected with electrostatically-formed nanowire sensor, *Sensors Actuators, B Chem.* 248 (2017) 240–246.  
doi:10.1016/j.snb.2017.03.150.
- [25] A. Henning, N. Swaminathan, Y. Vaknin, T. Jurca, K. Shimanovich, G. Shalev, Y. Rosenwaks, Control of the Intrinsic Sensor Response to Volatile Organic Compounds with Fringing Electric Fields, *ACS Sensors*. 3 (2018) 128–134.  
doi:10.1021/acssensors.7b00754.
- [26] S. Cristoloveanu, B. Blalock, F. Allibert, B. Dufrene, M. Mojarradi, The four-gate transistor, in: *Eur. Solid-State Device Res. Conf.*, IEEE Computer Society, 2002: pp. 323–326. doi:10.1109/ESSDERC.2002.194934.
- [27] G. Elias, T. Glatzel, E. Meyer, A. Schwarzman, A. Boag, Y. Rosenwaks, The role of the cantilever in Kelvin probe force: Microscopy measurements, *Beilstein J. Nanotechnol.* 2 (2011) 252–260. doi:10.3762/bjnano.2.29.
- [28] G. Cohen, E. Halpern, S.U. Nanayakkara, J.M. Luther, C. Held, R. Bennewitz, A. Boag, Y. Rosenwaks, Reconstruction of surface potential from Kelvin probe force microscopy images, *Nanotechnology*. 24 (2013). doi:10.1088/0957-4484/24/29/295702.
- [29] A. Kolmakov, D.O. Klenov, Y. Lilach, S. Stemmer, M. Moskovitst, Enhanced gas sensing by individual SnO<sub>2</sub> nanowires and nanobelts functionalized with Pd catalyst particles, *Nano Lett.* 5 (2005) 667–673. doi:10.1021/nl050082v.
- [30] J. Nah, S.B. Kumar, H. Fang, Y.Z. Chen, E. Plis, Y.L. Chueh, S. Krishna, J. Guo, A. Javey, Quantum size effects on the chemical sensing performance of two-dimensional semiconductors, *J. Phys. Chem. C*. 116 (2012) 9750–9754. doi:10.1021/jp300446z.
- [31] Z.H. Chen, J.S. Jie, L.B. Luo, H. Wang, C.S. Lee, S.T. Lee, Applications of silicon nanowires functionalized with palladium nanoparticles in hydrogen sensors, *Nanotechnology*. 18 (2007) 345502. doi:10.1088/0957-4484/18/34/345502.
- [32] K. Shimanovich, T. Coen, Y. Vaknin, A. Henning, J. Hayon, Y. Roizin, Y. Rosenwaks, CMOS Compatible Electrostatically Formed Nanowire Transistor for Efficient Sensing of Temperature, *IEEE Trans. Electron Devices*. 64 (2017) 3836–3840.  
doi:10.1109/TED.2017.2727548.
- [33] H. Kim, J. Yun, M. Gao, H. Kim, M. Cho, I. Park, Nanoporous Silicon Thin Film-Based

- Hydrogen Sensor Using Metal-Assisted Chemical Etching with Annealed Palladium Nanoparticles, *ACS Appl. Mater. Interfaces*. 12 (2020) 43614–43623. doi:10.1021/acsami.0c10785.
- [34] J. Baek, B. Jang, M.H. Kim, W. Kim, J. Kim, H.J. Rim, S. Shin, T. Lee, S. Cho, W. Lee, High-performance hydrogen sensing properties and sensing mechanism in Pd-coated p-type Si nanowire arrays, *Sensors Actuators, B Chem.* 256 (2018) 465–471. doi:10.1016/j.snb.2017.10.109.
- [35] M. Gao, M. Cho, H.-J. Han, Y.S. Jung, I. Park, Palladium-Decorated Silicon Nanomesh Fabricated by Nanosphere Lithography for High Performance, Room Temperature Hydrogen Sensing, *Small*. 14 (2018) 1703691. doi:10.1002/sml.201703691.
- [36] J.H. Ahn, J. Yun, D. Il Moon, Y.K. Choi, I. Park, Self-heated silicon nanowires for high performance hydrogen gas detection, *Nanotechnology*. 26 (2015) 095501. doi:10.1088/0957-4484/26/9/095501.
- [37] X. Tang, P.A. Haddad, N. Mager, X. Geng, N. Reckinger, S. Hermans, M. Debligny, J.P. Raskin, Chemically deposited palladium nanoparticles on graphene for hydrogen sensor applications, *Sci. Rep.* 9 (2019) 1–11. doi:10.1038/s41598-019-40257-7.
- [38] M. Ae Lim, D. Hwan Kim, C.-O. Park, Y. Wook Lee, S. Woo Han, Z. Li, R. Stan Williams, I. Park, A New Route toward Ultrasensitive, Flexible Chemical Sensors: Metal Nanotubes by Wet-Chemical Synthesis along Sacrificial Nanowire Templates, 13 (2020) 28. doi:10.1021/nn204009m.
- [39] J.H. Tsai, S.H. Liou, P.S. Lin, Y.C. Chen, InGaP/InGaAs field-effect transistor typed hydrogen sensor, *Appl. Surf. Sci.* 432 (2018) 224–227. doi:10.1016/j.apsusc.2017.03.246.
- [40] I. Darmadi, F.A.A. Nugroho, C. Langhammer, High-Performance Nanostructured Palladium-Based Hydrogen Sensors - Current Limitations and Strategies for Their Mitigation, *ACS Sensors*. (2020). doi:10.1021/acssensors.0c02019.
- [41] I. Lundström, M.S. Shivaraman, C. Svensson, Chemical reactions on palladium surfaces studied with Pd-MOS structures, *Surf. Sci.* 64 (1977) 497–519. doi:10.1016/0039-6028(77)90059-0.
- [42] I. Lundström, T. DiStefano, Hydrogen induced interfacial polarization at PdSiO<sub>2</sub> interfaces, *Surf. Sci.* 59 (1976) 23–32. doi:10.1016/0039-6028(76)90288-0.
- [43] Y. Irokawa, M. Usami, First-principles studies of hydrogen adsorption at Pd-SiO<sub>2</sub> interfaces, *Sensors (Switzerland)*. 15 (2015) 14757–14765. doi:10.3390/s150614757.
- [44] C. Quintanar, R. Caballero, M. Ugalde, M. Ramos, E. Chavira, H. Cruz-Manjarrez, F. Espinosa, Charge transfer and hydrogen adsorption in the Pd/Ag bimetallic nano system: an experimental and theoretical DFT cluster approach, *Mol. Phys.* 118 (2020) 1–10. doi:10.1080/00268976.2020.1820090.
- [45] J. Murakami, M. Futamata, Y. Nakao, S. Horiuchi, K. Bando, U. Nagashima, K. Yoshimura, Reduction of N<sub>2</sub> with H<sub>2</sub> on palladium surfaces at low temperatures, *Chem.*

Phys. Lett. 618 (2015) 1–5. doi:10.1016/j.cplett.2014.10.056.

- [46] N.M. Martin, M. Van Den Bossche, H. Grönbeck, C. Hakanoglu, J. Gustafson, S. Blomberg, M.A. Arman, A. Antony, R. Rai, A. Asthagiri, J.F. Weaver, E. Lundgren, Dissociative adsorption of hydrogen on PdO(101) studied by HRCLS and DFT, *J. Phys. Chem. C*. 117 (2013) 13510–13519. doi:10.1021/jp4036698.
- [47] N. Yamamoto, S. Tonomura, T. Matsuoka, H. Tsubomura, A study on a palladium-titanium oxide Schottky diode as a detector for gaseous components, *Surf. Sci.* 92 (1980) 400–406. doi:10.1016/0039-6028(80)90212-5.
- [48] J. Fogelberg, L.G. Petersson, Kinetic modelling of the H<sub>2</sub>-O<sub>2</sub> reaction on Pd and of its influence on the hydrogen response of a hydrogen sensitive Pd metal-oxide-semiconductor device, *Surf. Sci.* 350 (1996) 91–102. doi:10.1016/0039-6028(96)80059-8.
- [49] C. Hakanoglu, J.M. Hawkins, A. Asthagiri, J.F. Weaver, Strong kinetic isotope effect in the dissociative chemisorption of H<sub>2</sub> on a PdO(101) thin film, *J. Phys. Chem. C*. 114 (2010) 11485–11497. doi:10.1021/jp101715j.

## Figure captions:

**Fig. 1.** Illustration and characterization of the Pd-EFN device: (a) Schematic diagram of Pd-EFN device. (b) AFM image of the Pd-EFN channel with SiO<sub>2</sub> top oxide. (c) Zoomed-in AFM image of the Pd NPs in the marked area in (b) showing uniform distribution of the NPs. (d) Height profile of the Pd-NPs along the marked lines in (c) indicating particle size variation from 1 to 2 nm. (e) KPFM image of the marked area. (f) Contact potential difference (CPD) profile of the Pd-NPs along the marked lines in (e) at ground potential.

**Fig. 2.** Effect of Pd NPs decoration on electrical characteristics of the EFN device: (a)  $I_{DS}$ - $V_{BG}$  characteristics of the EFN device at  $V_{JG} = -2.5V$  and  $V_{DS} = 1V$  pre and post Pd NPs decoration. (b) Simulated electrostatic potential profile of the channel on Pd NPs decoration. With increase in number of Pd NPs the channel gets more depleted. Energy band alignment across the Pd-SiO<sub>2</sub>- $nSi$  showing (c) before and (d) after Pd NPs deposition. A depletion of channel near the SiO<sub>2</sub>/Si interface occurs after the Pd NPs deposition.

**Fig. 3.** Electrical characterization of the Pd-EFN device on H<sub>2</sub> exposure: (a) Typical  $I_{DS}$ - $V_{BG}$  characteristics of the Pd-EFN device for 0.4% H<sub>2</sub> exposure. On withdrawal of H<sub>2</sub> gas, the characteristics fully recover to these before sensing, indicating complete recovery. (b)  $I_{DS}$ - $V_{BG}$  characteristics of the Pd-EFN device at different  $V_{JG}$  and  $V_{DS} = 1V$  before and after 15 minutes exposure to 0.8% H<sub>2</sub>. The dotted lines indicate the curves obtained after exposure to H<sub>2</sub>. A negative shift in the threshold voltage ( $\Delta V_{Th}$  (BG)) occurs following H<sub>2</sub> exposure, which is equivalent to 'positive gating' of the channel. (c) Shift of back gate threshold voltages (with error bars) of the Pd-EFN device on sensing different concentrations of H<sub>2</sub> gas at different  $V_{JG}$  and a constant  $V_{DS}$  of 1V.

**Fig. 4.** Sensing behavior of Pd-EFN device: (a) Dynamic sensor responses of Pd-EFN device vs time towards different concentrations of H<sub>2</sub> at different V<sub>JG</sub> and a constant V<sub>DS</sub> = 1V with V<sub>BG</sub> = 0V. (b) Dynamic sensor response of the Pd-EFN device to varying concentrations of H<sub>2</sub> at V<sub>JG</sub> = -0.1V, V<sub>BG</sub> = -2V and V<sub>DS</sub> = 1V. A maximum sensor response of 2x10<sup>6</sup> is achieved at 0.8% H<sub>2</sub> exposure. (c) Plot of sensor response vs H<sub>2</sub> concentration of the Pd-EFN device with biasing conditions V<sub>JG</sub> = -0.1V, V<sub>BG</sub> = -2V and V<sub>DS</sub> = 1V. A linear fitting of the graph gives a sensitivity of ~400% ppm<sup>-1</sup> in the concentration range of 0.02 to 0.4%. (d) Cyclic response of Pd-EFN device towards 0.8% H<sub>2</sub> for 4 cycles demonstrating the reproducibility of the signal.

**Fig. 5.** Influence of temperature on the sensing performance metrics of the Pd-EFN device: (a) Dynamic sensor responses of Pd-EFN device vs time towards different concentrations of H<sub>2</sub> at different temperatures at constant V<sub>JG</sub> = -0.1V, V<sub>DS</sub> = 1V and V<sub>BG</sub> = 0V. (b) Plot of sensor response vs temperature at different H<sub>2</sub> concentrations. (c) Plot of response time vs H<sub>2</sub> concentration at 25 and 56 °C. (d) Plot of recovery time vs H<sub>2</sub> concentration at 25 and 56 °C.

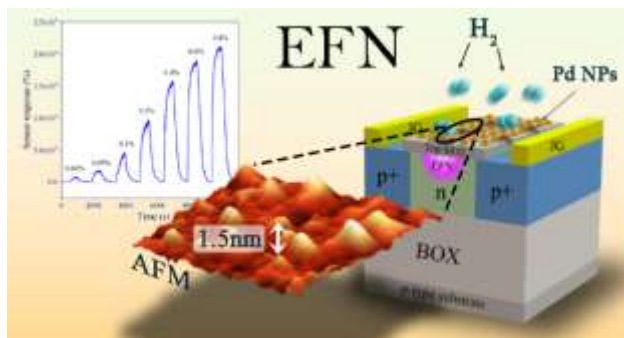
**Fig. 6.** Effect of relative humidity (30% and 50%) on (a) the dynamic sensor response of Pd-EFN at different H<sub>2</sub> concentrations at the same biasing conditions. Variation in current (log scale) of Pd-EFN device at different H<sub>2</sub> concentrations at (b) 0% RH (c) 30 % RH and (d) 50% RH at the same biasing conditions.

**Fig. 7.** Schematic of the model of interaction of H<sub>2</sub> with Pd-decorated EFN surface: (a) Adsorption of oxygen anions on surface of Pd NPs. (b) During initial H<sub>2</sub> exposure, removal of oxygen anions take place through formation of water creating more vacant sites for H<sub>2</sub> adsorption. (c) Adsorption and dissociation of H<sub>2</sub> on Pd into H atoms; they further diffuse into the interface of Pd and SiO<sub>2</sub> and induce dipoles. The H at the interface and surface are always in equilibrium. (d) On removal

of H<sub>2</sub>, the atomic H reaches the surface and due to dry air exposure, the oxygen molecules interact with them to form water thus facilitating desorption of H<sub>2</sub>. (e) On full recovery, initial conditions are restored.

**Fig. 8.** Energy band diagram across the Pd-SiO<sub>2</sub>-nSi (a) before and (b) after H<sub>2</sub> sensing. On H<sub>2</sub> sensing, the workfunction of Pd decreases contributing to increased current in the channel.

## Graphical abstract



Palladium nanoparticles (Pd NPs) decorated electrostatically formed nanowire (Pd-EFN) give an unprecedented sensitivity of  $\sim 2 \times 10^6$  % to 0.8%  $H_2$  exposure at room temperature. The catalytic properties of Pd NPs towards  $H_2$  in combination with the size tunable conducting channel of the EFN, defined post-fabrication by application of various surrounding gates, contribute to the drastically enhanced sensor performance metrics of the Pd-EFN sensor.

